Open Ceramics 16 (2023) 100472

Contents lists available at ScienceDirect

Open Ceramics

journal homepage: www.sciencedirect.com/journal/open-ceramics

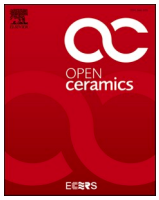

Stability assessment of alumina and SiC based refractories in a high temperature steam environment as potential thermal energy storage materials

N. Sena Yüzbasi *, Thomas Graule, Gurdial Blugan

Laboratory for High Performance Ceramics, Empa, Swiss Federal Laboratories for Materials Science and Technology, Dübendorf, 8600, Switzerland

ARTICLE INFO

Handling Editor: Dr P Colombo

ABSTRACT

Solar energy can be utilized not only for electricity generation but also for synthetic fuel production, making it a versatile option in the transition to a low-carbon and sustainable energy system. However, to enable economically viable solar fuel production, the development of efficient thermal energy storage (TES) materials is crucial. Ceramic materials have been identified as a potential solution for high-temperature TES applications. In this study, two commercially available refractories, alumina coated recrystallized silicon carbide and alumina-based refractory were investigated for their stability under long-term steam corrosion tests to evaluate their suitability as TES materials for a potential TES unit. X-ray diffraction (XRD) revealed that recrystallized silicon carbide is composed of two different SiC polytypes (moissanite 6H and moissanite 4H) while alumina-based refractory contained corundum and mullite. Upon being exposed to steam, both materials exhibited distinct characteristics. SiC experienced significant mass gain, a subtle lightning of its surface color and erosion of a porous alumina coating on the SiC. Amorphous silica phases were detected as an indication of oxidation of SiC from X-ray diffractograms. These remarkable changes clearly indicate that SiC is unsuitable for use in a potential thermal energy storage (TES) unit. On the other hand, there was no significant visual changes in the alumina-based refractory and the weight change was only marginal after corrosion tests. However, XRD indicated mullite completely disappeared after steam corrosion tests possibly due to its decomposition into Al_2O_3 and $Si(OH)_4$.

1. Introduction

Among renewable energy sources solar energy offers a sustainable, environmentally friendly, and economically viable solution to meet energy needs while reducing reliance on fossil fuels [1]. Concentrated solar power (CSP) plants convert sunlight into high-temperature heat, which can be used for solar thermochemical fuel production [2,3]. One of the key aspects to enable economically viable solar fuel production is the implementation of a thermal energy storage (TES) unit that enables stable and round-the-clock operation of thermochemical reactors which plays a crucial role in enhancing the efficiency and effectiveness of solar power systems [2–5]. Currently, in large-scale CSP systems, the most commonly utilized storage materials are synthetic oil and two tank molten salt systems, which function as sensible heat materials [6]. However, molten salts typically have temperature limitations typically between 200 °C and 600 °C [7–9]. At higher temperatures, some salts may start to decompose or exhibit unfavorable corrosive behavior, which can affect the performance and durability of the TES system. Therefore, molten salts are not suitable for high temperature applications, where temperatures can reach beyond 1000 °C specifically in solar tower systems [10], where the process heat generated from concentrated sunlight can be used for synthetic fuel production [11]. Therefore, there is an urgent need for development of new high TES materials taking into account the following requirements: (i) high thermal energy density in the storage material, (ii) compatible with the heat transfer fluid (HTF), (iii) high mechanical and chemical stability, (iv) withstanding numerous charging/discharging cycles, (v) low thermal losses and (vi) low cost and environmental impact [6,12].

In that context, ceramic materials are suggested to be a suitable option for high temperature applications while covering the requirements stated above. However, compared to molten salts (1.10–1.5 kJ/kg·K) or concrete (0.95 kJ/kg·K) most of the ceramic materials possess lower specific heat capacities (0.87 kJ/kg·K) [13]. Furthermore, ceramic or refractory materials such as magnesia or high alumina

* Corresponding author.
E-mail address: sena.yuezbasi@empa.ch (N.S. Yüzbasi).

https://doi.org/10.1016/j.oceram.2023.100472
Received 12 June 2023; Received in revised form 25 August 2023; Accepted 19 September 2023
Available online 2 October 2023

concrete [12] are stated to be highly cost competitive and can have complexities in shaping for effective distribution of heat in TES unit [10]. Solid materials like concrete and ceramics have been employed in two methods for heat exchange purposes: either as packed beds in conjunction with a suitable heat transfer fluid (HTF), or as monolithic blocks containing heat exchanger tubes [7,12,14].

For high temperature processes (1000 °C) suitable materials reported include alumina, magnesia, composites like high alumina concretes or clay ceramic with organic additives [12]. Aluminum oxide (Al_2O_3) and silicon carbide (SiC) widely used for high temperature refractory applications are particularly interesting candidates for serving as TES materials in CSP plants due to their specific properties that align well with the requirements of this application, as summarized briefly in Table 1 (properties of refractory ceramics are strongly dependent on their porosity and microstructure).

Although SiC is one of the outstanding candidates due to its high strength and stability at high temperatures, it also possesses exceptional thermal conductivity. This characteristic ensures rapid heat diffusion throughout the storage material, which is advantageous for energy storage. However, an excessively high thermal conductivity can also be a disadvantage as it can lead to rapid heat dissipation, quick and non-uniform heat distribution, creating hotspots near the heat source and significant heat losses to the surroundings. This can degrade the overall performance and causing instability in the storage system [19]. It is often beneficial to strike a balance between thermal conductivity and other properties like heat capacity, controllability of heat release and cost. In that context, alumina-based refractories can be suitable for TES applications due to its low cost, high availability, good thermal conductivity that can efficiently capture and release thermal energy during charging/discharging cycles.

To the best of our knowledge, these two materials have not been investigated under continuous steam exposure (when steam is used as heat transfer fluid (HTF)) at temperatures exceeding 1200 °C. Hence, in this study, we have investigated stability of recrystallized SiC and alumina-based refractory under long term steam corrosion tests to evaluate their applicability for a potential TES unit as a storage material.

2. Materials and methods

Refractories. Two different commercially available refractories (i) recrystallized silicon carbide (Morgan Advanced Ceramics Halsic R) coated with an alumina layer and (ii) fused corundum brick (alumina-based refractory) were used for corrosion testing. Alumina coating on SiC is often applied by several manufacturers to prevent adhesion and ceramics components from sticking to the refractory during the sintering process. This is important to ensure that the ceramics can be easily removed from the refractory after sintering without causing damage or deformation. Furthermore, the coating also acts as a barrier to prevent the diffusion of impurities, such as carbon (C) and other contaminants, from the refractory into the ceramic bodies being sintered. The main characteristics of the raw materials are presented in the results section. Materials were cut to 25 x 25 × 7 mm for corrosion tests in a specially adapted tubular furnace.

Table 1
A brief comparison of properties of alumina-based and SiC refractories.

	Alumina-based refractories	Silicon Carbide (SiC)
High temperature stability	✔	✔
Specific heat capacity [12,15]	~800–940 J/kg K	650–1040 J/kg K
Thermal conductivity [15–17]	2–30 W/m-K	30–200 W/m-K
Thermal cycling performance	Good	Excellent
Chemical compatibility	Good	Good
Mean thermal expansion coefficient (20–1000 °C, 10^{-6}/K) [15,18]	7.4–9	3.7–5
Durability	✔	✔
Compressive strength (MPa) [15]	300–4500	1200–3600
Compatibility with heat transfer fluid	Depending on use	Depending on use

Corrosion testing. The oxidation corrosion testing was conducted in a Carbolite STF 16/61 tube furnace (Neuhausen, Germany). Fig. 1a shows fiber plugs with a central alumina pipe that has an internal diameter 20 mm located in the custom made inlet flange. The central pipe of the flange is made of Alloy 600 and longer than the fiber plug for an effective steam delivery. Fig. 1b shows the steam production unit. The steam corrosion tests were performed at 1250 °C. Prior to testing, the furnace was heated up to 1250 °C with a 1.5 K/min heating rate. After reaching the operation temperature ultrapure water (MicroPure UV System, Thermo Scientific, Waltham, Massachusetts, USA) was fed to a round bottom flask standing on an electrical heating mantle using a peristaltic pump. Steam production with this method could be successfully achieved and delivered to the tube furnace though the inlet flange described above. At the outlet, steam was condensed and collected in a gas wash bottle as shown in Fig. 1c. The flowrate of the water was fixed to approximaterly 2.7 ml/min. For real time monitoring of the temperature in the furnace during the corrosion tests, the temperature inside the furnace was continuously monitored via S-type thermocouple (JUMO Mess-und Regeltechnik AG, Stäfa, Switzerland) which was installed from the end flange of the tube shown in Fig. 1c and d. The temperature data collection was measured every 5 s and recorded with a USB-2001-TC data acquisition (DAQ) device from MC Measurement Computing Company (Massachusetts, USA). Temperature changes at the metal part of the inlet and outlet flanges were recorded (every 2 min) using K-type thermocouples (Testo AG Mönchaltorf, Switzerland) during blank run. The maximum temperature was below 90 °C and fairly stable in both of the flanges after steam flow was started. ~65 wt % of the water that was fed to furnace was collected in the condenser unit at the outlet.

The refractory specimens were located in alumina crucibles filled with coarse alumina acting as a powder bed to avoid contamination or sticking of the refractory cuts on the crucibles (Fig. 1d). In a typical testing, materials were exposed to steam around 80 h, followed by cooling down the furnace and photographing, weighing and measuring the dimensions of the tested specimens in order to trace the changes in the material e.g. color change, weight and expansion/shrinkage trends. Steam corrosion tests were continued until 500 h of steam exposure was reached based on the standard test method for evaluating oxidation resistance of silicon carbide (ASTM C863).

2.1. Characterization

The X-ray diffraction (XRD) analysis of the crystalline phases in the refractory materials was conducted using the PANalytical X'Pert PROh–2h (PANalytical, Netherlands) scan system equipped with a Johansson monochromator (Cu Kα1 radiation, 1.5406 Å) and a X'Celerator linear detector. The scans were collected in the 2θ range of 5–80° with a step size of 0.016° and a scanning speed of 0.021° s−1 56. The HighScore Plus Software was employed to analyze the phase compositions of the spectra.

The surface and sub-surface morphology of the materials were assessed using scanning electron microscopy (SEM) with a Tescan SEM VEGA3 instrument from Tescan Instruments (Brno, Czech Republic). For cross-sectional imaging, the refractories were ground and polished approximately 2 mm. To evaluate elemental mapping, energy-dispersive X-ray spectroscopy (EDX) analysis was performed using Bruker's XFlash 6 detector from Bruker Nano GmbH (Berlin, Germany).

3. Results and discussion

3.1. Characterization of the starting refractories

Fig. 2 shows the X-ray diffraction (XRD) patterns of the fresh

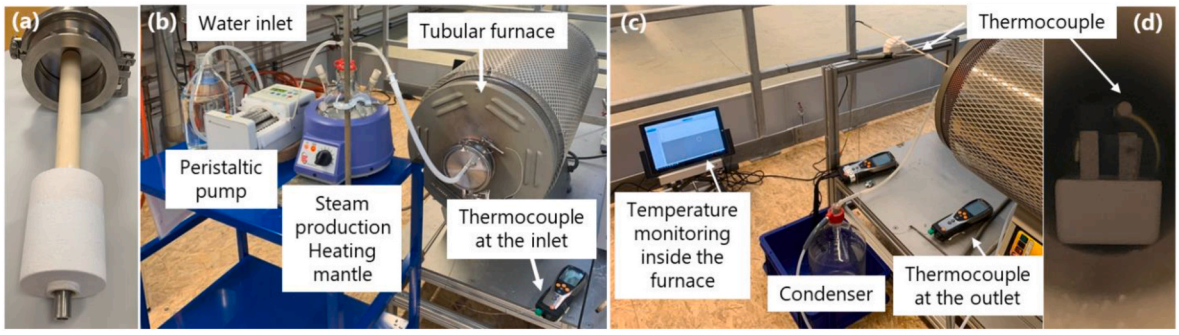

Fig. 1. Steam corrosion test rig (a) Fibre plug inside the inlet flange, (b) steam production unit connected to inlet flange and (c) outlet flange and condenser unit and (d) alumina boat located inside the furnace together with thermocouple.

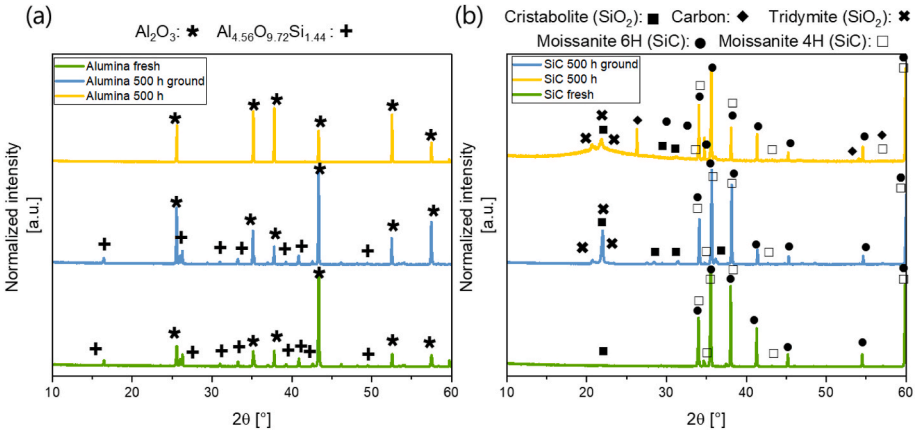

Fig. 2. XRD diffraction patterns of (a) alumina-based and (b) SiC refractories before and after 500 h of corrosion tests.

materials and after 500 h of corrosion testing. XRD spectrum of alumina-based refractory indicates the presence of two crystalline phases i.e. α-Al_2O_3 (corundum, ICSD collection code: 160604) and $Al_{4.56}Si_{1.44}O_{9.72}$ (mullite, ICSD collection code: 156191) in the fresh state. This is typical for commercial grades of alumina-based refractory materials, which are often made from fused Al_2O_3, fused SiO_2 and mullite starting materials. In the case of recrystallized SiC, two different SiC polytypes were determined. The main crystalline phase was moissanite 6H (SiC(6H), ICDS collection code: 15325) with an overlap of the Bragg reflections from moissanite 4H (SiC(4H), ICDS collection code: 24170). Additionally, very weak peaks of cristabolite (SiO_2, ICSD collection code: 34931) were also detected as an indicative of the thin layer of SiO_2 always present on the surface of the starting SiC powder and contributing to the liquid phase sintering.

Fig. 3 shows the surface morphology and elemental mappings of the materials together with the optical microscopy images in their fresh state. One side of the recrystallized SiC was coated with a porous white alumina layer by the manufacturer. This is confirmed with elemental mapping given in Fig. 3a. Silicon was also detected in the EDX maps of the alumina coating. Electron micrographs indicate the coating is not a fully dense layer, rather possessing porous structure and rough morphology. Higher magnification micrographs shows the presence of inhomogeneous grain sizes. Fig. 3b shows the uncoated black SiC side. Both electron and optical microscopy images show that this material has relative high-density for a refractory material (2.70–3.10 g/cm^3, as provided in the datasheet) as well as some open porous structure. EDX mappings indicate the presence of carbon, silicon and oxygen. Small quantities of oxygen given in Table 2 indicates the partial oxidation of the SiC on the surface in line with the findings in XRD with the presence of weak cristobalite peaks. Oxygen is mainly accumulated at the edges of the open pores.

In the case of alumina presented in Fig. 4, the segregation of the mullite and corundum is clearly demonstrated in the elemental maps. Fine mullite particles observed to be homogenously spread in between the large alumina grains in the fresh state.

3.2. Steam corrosion testing

The selected refractories placed in an alumina boat at the standing position before corrosion tests are shown in Fig. 1d. The gradual visual changes in the SiC and alumina-based refractories for both sides are shown in Fig. 5a and b, respectively. In the case of alumina-based refractory, there was not a significant visual change in the material on both sides except the slight color change. Fig. 5c compares the alumina-based refractory before and after corrosion tests and pink coloration over time is visible upon 550 h of steam exposure. This color change may be correlated with the accumulation of chromium on alumina that is expected to be released as a result of degradation of the Alloy 600 tube of the inlet flange (located at the heating zone of the tube furnace) [20]. Alloy 600 is rich in chromium (~15 wt%) and might have led to formation of some ruby, a form of aluminum oxide doped with chromium that is known to have the pink color at low doping [21].

In the case SiC the alumina coating started to diminish already after 50 h. This indicates that steam flow causes high temperature erosion on the porous alumina coating and the rest of the alumina coat showed tendency to coalescence and formed small bubbles in a distributed manner. Erosion induced breakdown of oxide layers in corrosive environments is often observed in steam turbines [22]. Furthermore, after 245 h of steam exposure the tested specimens were sticking on to alumina coarse grain sand possibly due to the formation and outward release of the glassy phases during corrosion tests. Strong bonding of SiC on alumina coarse sand was observed in each cycle. After 500 h of steam

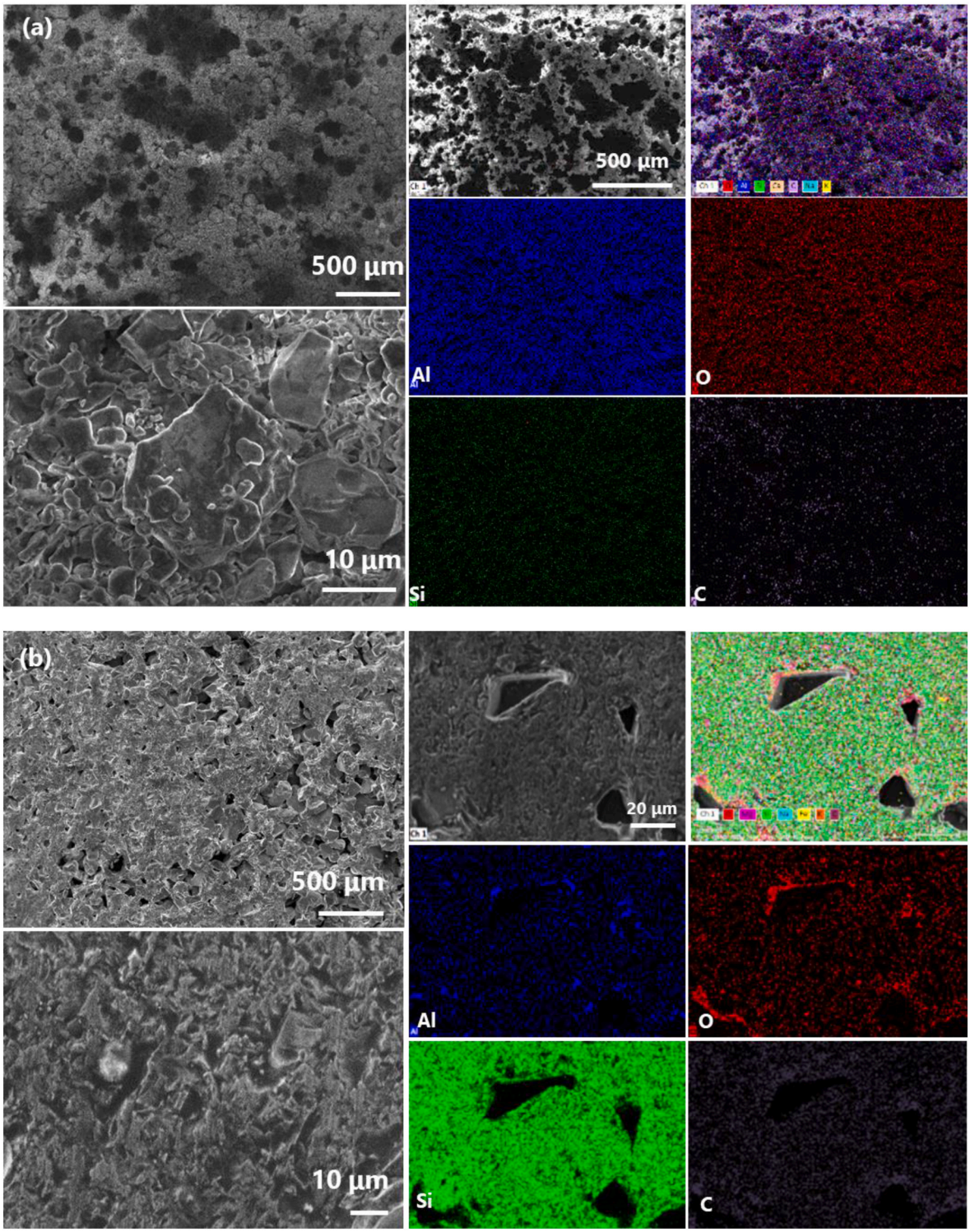

Fig. 3. SEM, EDX elemental mapping and optical microscopy images of (a) alumina coated side of SiC, (b) uncoated black side of the SiC refractory.

exposure alumina coating was observed to be completely destroyed. SiC/SiC ceramic matrix composites are mostly used in turbine engines as well as space vehicles that often experience erosion ending up with a substantial removal of material more dramatically at elevated temperatures [23]. Eventually, the black surface of the SiC refractory exhibited a subtle lightning, while the prominence of the gray color became more noticeable.

Fig. 6 demonstrates the mass change with the specimens during corrosion test cycles. There was a sharp increase in the mass of SiC up to 3.5 wt% mass gain upon steam exposure at 1250 °C. Mass gain reached its maximum peak point at around 250 h and started to decrease down to 2 wt% of total mass gain at the end of the corrosion testing. Regarding alumina, the material exhibited a relatively stable condition, with only a minimal increase in weight, around 0.28% by weight.

3.3. Characterization of the refractories after steam corrosion tests

After conducting steam corrosion tests, refractories were further

Table 2
Elemental composition of the refractories in atomic %.

atom %	Al	Si	O	C	Na	Ca	K	Mg	Cr	Ti	Fe
SiC fresh	0.13	22.79	8.34	68.43	0.16	N.A.	0.07	0.02	N.A.	N.A.	N.A.
SiC fresh (alumina coat)	20.78	2.33	54.99	20.99	0.3	0.26	N.A.	0.22	0.01	0.01	0.04
Alumina fresh	24.31	5.49	68.46	N.A.	0.84	0.31	0.13	0.39	N.A.	0.04	0.02
SiC after 500 h	0.32	36.8	22.25	40.08	0.19	0.18	0.01	0.14	N.A.	0.01	0.01
SiC after 500 h – (magnified)	0.32	38.19	21.87	38.95	0.21	0.23	N.A.	0.17	0.01	N.A.	0.02
SiC after 500 h (alumina coat)	3.88	22.23	61.54	7.78	3.38	0.18	0.13	0.1	0.19	0.02	0.06
Alumina after 500 h	28.5	5.5	62.45	N.A.	2.25	0.51	0.15	0.4	0.05	0.09	0.09

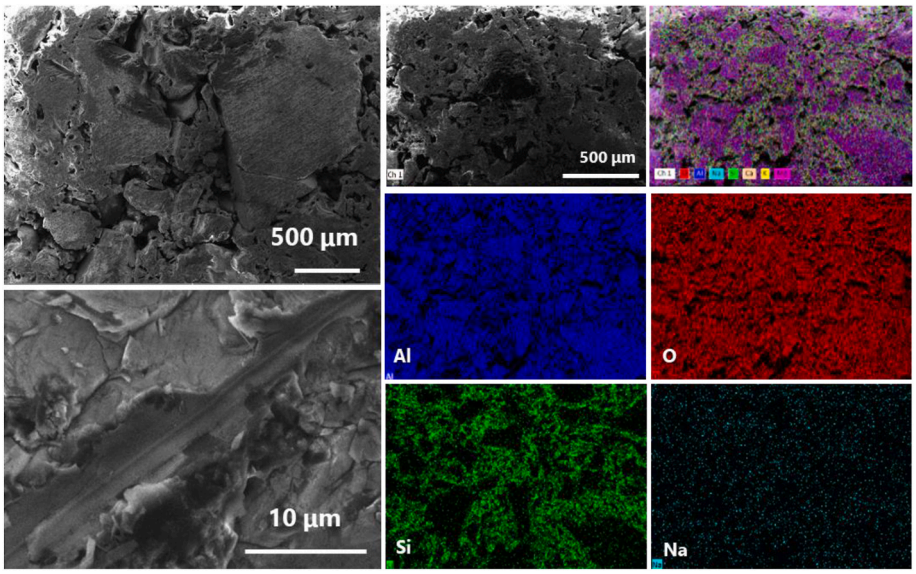

Fig. 4. SEM, EDX elemental mapping and optical microscopy images of alumina-based refractory in their fresh state.

characterized by means of XRD and SEM/EDX. Additionally, tested specimens were surface ground 2 mm with a diamond wheel from one side to evaluate the changes occurring in the subsurface and are shown in Figs. 7 and 8. Electron micrographs revealed that the morphology of the alumina coat which formerly possessed a rough morphology in its fresh state changed significantly after steam exposure. The micrograph of the eroded surfaces with the coating revealed the presence of crater-like formations as seen in Fig. 7a. In line with the visual observations, Table 2 indicates that the alumina fraction in the coated side significantly decreased as indicative of removal of the alumina coating. A notable finding from the elemental mapping analysis was the elevated sodium content observed following 500 h of exposure to steam.

Regarding the black side of the SiC material showed that the oxygen content increased while the carbon content decreased (Table 2). These changes suggest that oxidation has occurred which also explains the significant mass gain given in Fig. 6. This is further confirmed with diffraction patterns given in Fig. 2.

In addition to SiC polytypes, moissanite 6H (SiC(6H) and moissanite 4H (SiC(4H), the presence of amorphous high temperature polymorphs of silica phases such as cristobalite and tridymite (SiO_2, ICSD collection code: 1440) and cristobalite (SiO_2, ICSD collection code: 34931) together with carbon (ICSD collection code: 29123) after corrosion tests. Bright spots detected in the electron micrographs as depicted in Fig. 4b are SiO_2 phases formed upon oxidation based on the analysis of the elemental maps. SiO_2 are composed of small grains when compared to SiC and distributed across the surface. Cristobalite and tridymite are typically characterized by the arrangement of silica tetrahedra in either a two-layer structure (tridymite) or a three-layer structure (cristobalite) [24]. Electron micrographs indicated that the pores of SiC were disappearing as SiO_2 transformed into a molten state with sufficient fluidity and filled the cracks and pores during the high temperature steam corrosion tests [25]. Based on the mass gain profile given in Fig. 5, after 250 h the decrease in the mass upon steam exposure maybe correlated with the formation of an adherent passivating layer of SiO_2 that prevents further oxidation as a result of the low diffusivity of the oxygen into the interior of SiC [25,26]. The XRD spectrum of the ground sample, however, indicates that the refractory specimen was already inherently oxidized due to the presence of cristobalite and tridymite. However, no amorphous phases were detected at the subsurface.

In the case of alumina-based refractory, there were only marginal changes in the surface and subsurface morphology upon steam exposure. After 500 h, mullite phase was observed to be completely diminished and decomposed into alumina and orthosilicic acid phase as can be seen from Fig. 2a according to Equation (1), which is in line with the findings of Ueno et al. [27].

$$Al_6Si_2O_{13}(s) + 4H_2O(g) = 3Al_2O_3(s) + 2Si(OH)_4(g) \quad (1)$$

Removal of silica was expected to result in mass loss in Fig. 6, however, a completely opposite trend i.e. mass gain, was observed which can be explained by the diffusion of water vapor into alumina lattice in the water vapor environment [27]. Furthermore, silicon containing phases were not detected in XRD, however, EDX maps shown in Fig. 8 still showed the presence of some silicon. Compared to its fresh state, however, silicon was not homogenously segregated between the large alumina grains but rather aggregated and accumulated on the alumina grains after cyclic steam corrosion tests, suggesting some thermal diffusional effects.

4. Conclusions

This study focused on assessing the stability of ceramic-based

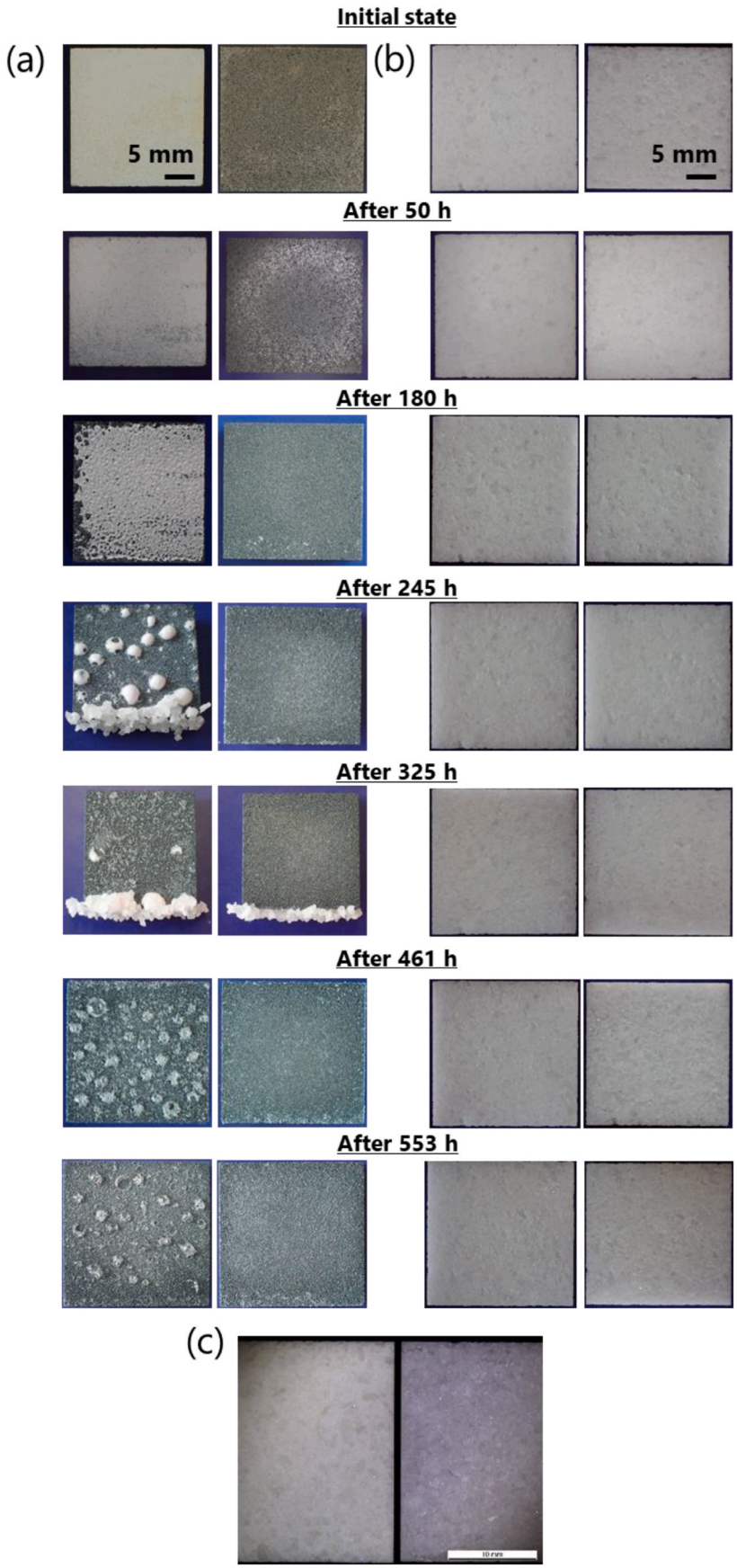

Fig. 5. Gradual degradation of (a) SiC refractory and (b) alumina-based refractory on both surfaces upon steam corrosion testing over time and (c) comparison of alumina-based refractory before (left) and after (right) corrosion tests.

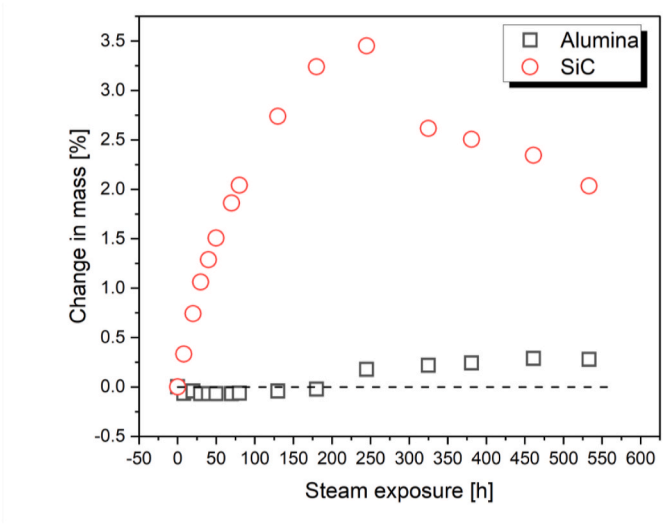

Fig. 6. Weight changes of the refractories during steam corrosion tests.

thermal energy storage (TES) materials that demonstrate compatibility with high temperatures (~1200 °C) and possess the capability to endure numerous heat charging/discharging cycles while utilizing steam as the heat transfer fluid. To accomplish this, a comprehensive analysis was conducted utilizing alumina coated recrystallized SiC and alumina-based refractory before and after undergoing corrosion tests of 500 h. Recrystallized SiC, while known for being a high-performance refractory material, demonstrated unsuitability for the specified high-temperature and high-humidity conditions. It experienced excessive mass changes (up to 2 wt% mass gain) and underwent phase changes as a result of its reactions with steam, likely leading to a degradation in its properties over time. In contrast, the alumina-based refractory exhibited more favorable characteristics. It demonstrated lower mass change (0.28 wt% mass gain) and displayed a reduced tendency to generate new reaction products within the given test environment. However, the mullite presenting in the fresh state of the alumina-based refractory diminished possibly due to its decomposition into alumina and orthosilicic acid in steam environment. Also, reaction with possible metallic ions present in a high temperature steam environment may occur as observed with chromium. Overall, alumina-based material could be a promising option for further investigation as a high temperature TES material.

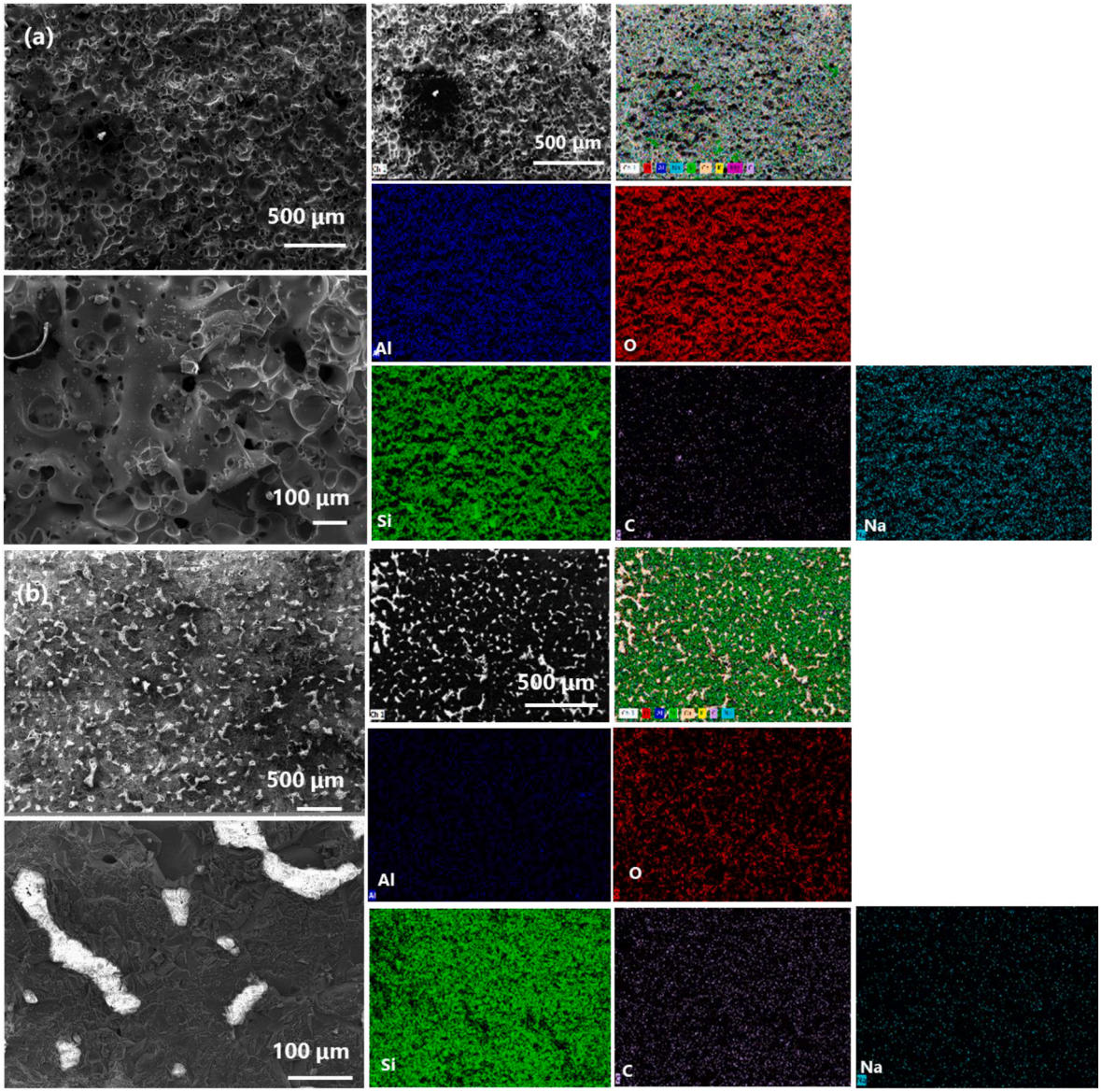

Fig. 7. SEM and EDX elemental mapping of (a) alumina coated side of SiC and (b) uncoated black side of the SiC refractory after 500 h of corrosion testing.

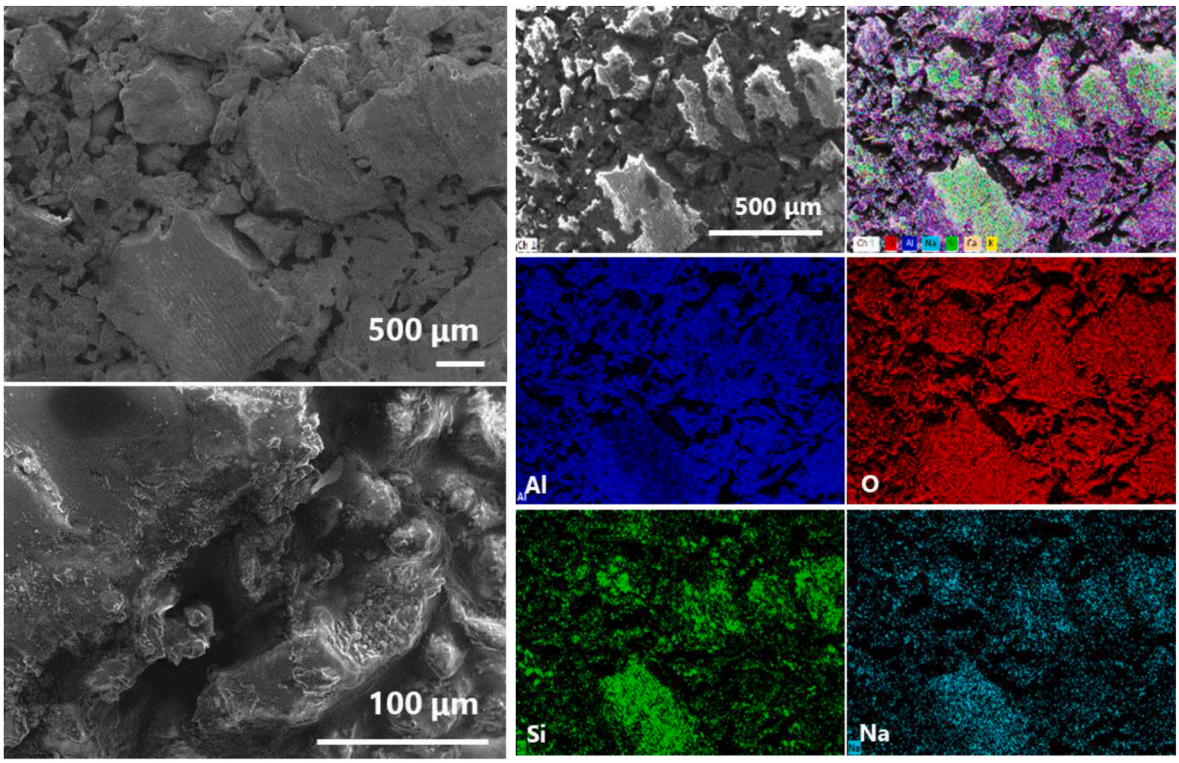

Fig. 8. SEM and EDX elemental mapping of alumina-based refractory after 500 h of corrosion testing.

Declaration of competing interest

The authors declare that they have no known competing financial interests or personal relationships that could have appeared to influence the work reported in this paper.

Acknowledgments

The authors would like to acknowledge the Swiss Innovation Agency-Innosuisse for funding this work as part of project 53851.1 IP-EE. We would also like to thank Ardian Salihu from Empa's laboratory of Mechanical Engineering for design and evaluation of parts for the corrosion furnace construction.

References

[1] C.F. Shih, T. Zhang, J. Li, C. Bai, Powering the future with liquid sunshine, Joule 2 (10) (2018) 1925–1949.
[2] W.C. Chueh, C. Falter, M. Abbott, D. Scipio, P. Furler, S.M. Haile, A. Steinfeld, High-flux solar-driven thermochemical dissociation of CO2 and H2O using nonstoichiometric ceria, Science 330 (6012) (2010) 1797–1801.
[3] M. Romero, A. Steinfeld, Concentrating solar thermal power and thermochemical fuels, Energy Environ. Sci. 5 (11) (2012) 9234–9245.
[4] L. Geissbühler, A. Mathur, A. Mularczyk, A. Haselbacher, An assessment of thermocline-control methods for packed-bed thermal-energy storage in CSP plants, Part 1: method descriptions, Sol. Energy 178 (2019) 341–350.
[5] M. Liu, N.S. Tay, S. Bell, M. Belusko, R. Jacob, G. Will, W. Saman, F. Bruno, Review on concentrating solar power plants and new developments in high temperature thermal energy storage technologies, Renew. Sustain. Energy Rev. 53 (2016) 1411–1432.
[6] S. Kuravi, J. Trahan, D.Y. Goswami, M.M. Rahman, E.K. Stefanakos, Thermal energy storage technologies and systems for concentrating solar power plants, Prog. Energy Combust. Sci. 39 (4) (2013) 285–319.
[7] A. Gil, M. Medrano, I. Martorell, A. Lázaro, P. Dolado, B. Zalba, L.F. Cabeza, State of the art on high temperature thermal energy storage for power generation. Part 1—concepts, materials and modellization, Renew. Sustain. Energy Rev. 14 (1) (2010) 31–55.
[8] M. Medrano, A. Gil, I. Martorell, X. Potau, L.F. Cabeza, State of the art on high-temperature thermal energy storage for power generation. Part 2—case studies, Renew. Sustain. Energy Rev. 14 (1) (2010) 56–72.
[9] S.S. Mostafavi Tehrani, R.A. Taylor, K. Nithyanandam, A. Shafiei Ghazani, Annual comparative performance and cost analysis of high temperature, sensible thermal energy storage systems integrated with a concentrated solar power plant, Sol. Energy 153 (2017) 153–172.
[10] A.R. Sane, D. Pham Minh, N. Semlal, R. Boulif, C. Toussaint, A. Germeau, A. Nzihou, Clay/phosphate-based ceramic materials for thermal energy storage – Part I: effect of synthetic phosphate content on microstructure, thermo-physical and thermo-mechanical properties, Open Ceramics 14 (2023), 100346.
[11] R. Schäppi, D. Rutz, F. Dähler, A. Muroyama, P. Haueter, J. Lilliestam, A. Patt, P. Furler, A. Steinfeld, Drop-in fuels from sunlight and air, Nature 601 (7891) (2022) 63–68.
[12] S. Khare, M. Dell'Amico, C. Knight, S. McGarry, Selection of materials for high temperature sensible energy storage, Sol. Energy Mater. Sol. Cell. 115 (2013) 114–122.
[13] P.M. Nigay, A. Nzihou, C.E. White, W.O. Soboyejo, Structure and properties of clay ceramics for thermal energy storage, J. Am. Ceram. Soc. 100 (10) (2017) 4748–4759.
[14] R. Tamme, U. Taut, C. Streuber, H. Kalfa, Energy storage development for solar thermal processes, Sol. Energy Mater. 24 (1) (1991) 386–396.
[15] D. Munz, T. Fett, Ceramics: Mechanical Properties, Failure Behaviour, Materials Selection, Springer Science & Business Media, 1999.
[16] W. D-Pabst, E. Gregorová, Effective Thermal and Thermoelastic Properties of Alumina, Zirconia and Alumina-Zirconia Composite Ceramics, New Developments in Materials Science Research, Nova Science, New York, 2007, pp. 77–138.
[17] S. Perevislov, E. Motaylo, E. Novoselov, D. Nesmelov, Thermal conductivity of SiC-B4C materials obtained by reaction-sintering method, in: IOP Conference Series: Materials Science and Engineering, IOP Publishing, 2020, 012066.
[18] W. Kingery, H. Bowen, D. Uhlman, Introduction to Ceramics, second ed.ed, John Wiley and Sons Inc 303, USA, 1967.
[19] M.I. Khan, F. Asfand, S.G. Al-Ghamdi, Progress in research and technological advancements of thermal energy storage systems for concentrated solar power, J. Energy Storage 55 (2022), 105860.
[20] C. Fujii, R. Meussner, The mechanism of the high-temperature oxidation of iron-chromium alloys in water vapor, J. Electrochem. Soc. 111 (11) (1964) 1215.
[21] P. Berdahl, S.S. Chen, H. Destaillats, T.W. Kirchstetter, R.M. Levinson, M.A. Zalich, Fluorescent cooling of objects exposed to sunlight – the ruby example, Sol. Energy Mater. Sol. Cell. 157 (2016) 312–317.
[22] S. Matthews, B. James, M. Hyland, High temperature erosion–oxidation of Cr3C2–NiCr thermal spray coatings under simulated turbine conditions, Corrosion Sci. 70 (2013) 203–211.
[23] R.P. Panakarajupally, F. Mirza, J. El Rassi, G.N. Morscher, F. Abdi, S. Choi, Solid particle erosion behavior of melt-infiltrated SiC/SiC ceramic matrix composites (CMCs) in a simulated turbine engine environment, Compos. B Eng. 216 (2021), 108860.
[24] M.d.C. Gutiérrez-Castorena, W.R. Effland, 21 - pedogenic and biogenic siliceous features, in: G. Stoops, V. Marcelino, F. Mees (Eds.), Interpretation of Micromorphological Features of Soils and Regoliths, Elsevier, Amsterdam, 2010, pp. 471–496.

[25] M.W. Chen, H.P. Qiu, J. Jiao, Y. Wang, W.J. Xie, High Temperature Oxidation Behavior of Silicon Carbide Ceramic, Key Engineering Materials, Trans Tech Publ, 2016, pp. 89–92.

[26] M. Yoshimura, J.-i. Kase, S. Sōmiya, Oxidation of SiC powder by high-temperature, high-pressure H2O, J. Mater. Res. 1 (1) (1986) 100–103.

[27] S. Ueno, T. Ohji, H.-T. Lin, Corrosion and recession of mullite in water vapor environment, J. Eur. Ceram. Soc. 28 (2) (2008) 431–435.